*Int. J. Electrochem. Sci.*, 15 **(2020)** 2335 – 2353, doi: 10.20964/2020.03.73

International Journal of
ELECTROCHEMICAL
SCIENCE
www.electrochemsci.org

# Corrosion Inhibition Effect of Cefotaxime Sodium on Mild Steel in Acidic and Neutral Media

*Bilan Lin*[1,2,*] , *Shiwei Zheng*[1], *Jiapo Liu*[1], *and Yuye Xu*[3]

[1] School of Material Science and Engineering, Xiamen University of Technology, Xiamen 361024, China
[2] Key Laboratory of Functional Materials and Applications of Fujian Province, Xiamen 361024, China
[3] College of Civil Engineering, Huaqiao University, Xiamen, Fujian 361021, China
[*]E-mail: linbilan@xmut.edu.cn

*Received:* 15 November 2019 / *Accepted:* 5 January 2020 / *Published:* 10 February 2020

The expired antibiotic cefotaxime sodium (CEF) was investigated as a corrosion inhibitor for mild steel in 1.0 mol/L $H_3PO_4$ and 0.6 mol/L NaCl solutions. Corrosion behavior was studied via the open circuit potential (OCP), potentiodynamic polarization curves, electrochemical impedance spectroscopy (EIS), and scanning electron microscopy. Furthermore, the adsorption mechanism was investigated. In $H_3PO_4$ solution, the adsorption-desorption equilibrium of CEF molecule was reached rapidly. CEF acted as a mixed corrosion inhibitor. CEF adsorption obeyed Langmuir isotherm model and could be attributed primarily to chemical adsorption. The optimal concentration of CEF was in the range of 0.5 m mol/L and 0.8 m mol/L and the geometric coverage was about 0.87. A continuous thin film formed and the double-layer capacitance decreased. CEF offered effective long-term corrosion protection for mild steel in $H_3PO_4$ solution. However, the CEF adsorption-desorption equilibrium in NaCl solution was difficult. CEF could only slightly inhibit anodic corrosion. The CEF coverage was only 0.1. CEF provided almost no corrosion protection in the neutral NaCl solution. CEF did not change the corrosion mechanism of mild steel. The contrast inhibition efficiency between both solutions is directly related to the different corrosion mechanisms and the large quantity of chloride ions present in NaCl solution.

**Keywords:** Cefotaxime; Mild Steel; Corrosion; Electrochemical; Expired Drugs

## 1. INTRODUCTION

Because of its excellent performance and low cost, mild steel has been widely used for the construction of pressure vessels, pipelines, and ships [1, 2]. However, its corrosion resistance is impaired under acidic and corrosive environments. Commonly used anti-corrosion measures include coatings, anodic protection, cathodic protection, and corrosion inhibitors [3-5]. Among these, corrosion

inhibitors are economical, effective, and convenient [6-8]. Corrosion inhibitors may be organic or inorganic, and are classified according to their chemical composition. Inorganic inhibitors such as chromate, nitrite, molybdate, and tungstate are effective but toxic, so much of them do not meet the environmental requirements and are restricted. Recently, many attentions have been performed to investigate corrosion protection using organic inhibitors [9-11]. Hassan et al. [12] comparatively investigated the inhibition and adsorption behaviors of triazole derivatives for carbon steel in HCl solutions; and found that the derivatives exhibited mixed adsorption mechanism and acted as mixed inhibitors. Guo et al. [13] found that the corrosion inhibition of carbon steel in HCl solution by 3-butyl-5,5-dimethyl hydantoin imidazole quaternary ammonium salt increased with the inhibitor concentration, and the adsorption mode could be described by Langmuir isotherm model. Ahamad et al. [14] found that bis(benzimidazol-2-yl) disulfide provided good protection against corrosion for carbon steel in both HCl and $H_2SO_4$ solutions, although the protective action was more effective in the latter. Recently, organic compounds extracted from plants have also been attempted to use as corrosion inhibitors for metals in acidic media and can also provide good corrosion inhibition. Zhang et al. [15] used a margarita suffruticosa extract as a corrosion inhibitor for carbon steel in HCl solution. They showed that it was a mixed corrosion inhibitor with main control of the cathode, and the inhibition mechanism could be attributed to the geometric coverage effect of the extract. Chen et al. [16] found that an extract of sargassum japonica inhibited the corrosion of carbon steel in HCl solution, and it could be described by both the Langmuir and Dhar-Flory-Huggins adsorption models. Singh et al. [17] showed that the extracts of andrographis paniculata, nux vomica, moringa, and bacopa monnieri also provided corrosion protection for steel in HCl solution via adsorption.

Studies have shown that organic molecules used as medical drugs possess heteroatoms such as N, O, and S. Therefore, they have polar groups and heterocyclic structures that can adsorb on the metal surface or chelate with metal atoms [18]. Expired organic clinical drugs have attracted interest as potential corrosion inhibitors [19-21]. Nathiya et al. [22] investigated the protective effect of expired moxifloxacin and polyol against the corrosion of aluminium alloy in $H_2SO_4$ solutions via weight loss, polarization, and EIS measurements; they showed that both drugs were mixed inhibitors and the adsorption followed Langmuir model. Anaee et al. [23] found that the adsorption of expired etoricoxib on the carbon steel surface in $H_3PO_4$ was a mixed mode, with mainly chemical adsorption. The corrosion inhibition efficiency of the expired isoniazid for carbon steel in HCl solution was larger than 90%, with a mixed inhibition mechanism [24]. While expired tramado mainly suppressed the cathodic corrosion of carbon steel in HCl [25]. Expired cefadroxil and clomethocillin were shown to greatly inhibit the anodic corrosion of 6063 aluminum alloy in $HNO_3$ media [26].

The corrosion inhibition of expired drugs for metals in neutral media has rarely been described in recent literature. In this work, expired cefotaxime sodium (CEF) was used as a corrosion inhibitor for mild steel in both neutral NaCl and acidic $H_3PO_4$ solutions. Measurements of OCP, potentiodynamic polarization, and EIS were carried out. The adsorption mode and thermodynamic parameters were analyzed and the inhibition mechanism was discussed.

## 2. EXPERIMENTAL

### *2.1 Materials and reagents*

Mild steel samples (1 cm × 1 cm × 0.3 cm) were used as test materials. The chemical composition was as follows (mass fraction, %): 0.13 C, 0.02 Si, 0.38 Mn, 0.014 P, and 0.031 S, with the balance Fe. The working area was 1.0 $cm^2$. The untested portion was sealed with epoxy resin.

The molecular formula and molecular weight of cefotaxime sodium were $C_{16}H_{17}N_5O_7S_2$ and 455.5, respectively. Its structural formula is depicted in Fig. 1.

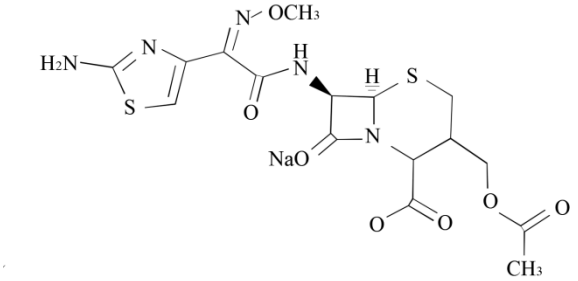


**Figure 1.** CEF chemical structure.

For measurements, 85% $H_3PO_4$ (mass fraction, %) was diluted into 1.0 mol/L $H_3PO_4$ solution and CEF was subsequently added. The CEF concentrations tested were 0 m mol/L, 0.01 m mol/L, 0.05 m mol/L, 0.10 m mol/L, 0.50 m mol/L, 0.80 m mol/L, and 1.0 m mol/L, respectively.

The concentration of NaCl was 3.5% (mass fraction), i.e., 0.6 mol/L, and the CEF concentrations tested were 0 mg/L, 50 mg/L, 100 mg/L, 300 mg/L, 500 mg/L, and 1000 mg/L, respectively.

### *2.2 Electrochemical measurements*

Electrochemical measurements were performed using a CHI604E electrochemical workstation. The test system was a conventional three-electrode apparatus. The working, reference, and auxiliary electrodes corresponded to the measured mild steel electrode, the saturated calomel electrode (SCE), and a platinum electrode, respectively. Before the electrochemical tests, the working surface of mild steel was polished sequentially with pieces of sandpaper from No. 200 to No. 2000 and then scrubbed with acetone, rinsed with distilled water, and dried in cool air.

The OCP was monitored for 1 h after the mild steel electrode was immersed in the corrosive solution. It was observed that the system was mostly stable. EIS diagrams and potentiodynamic polarization curves were measured sequentially.

The initial and final potentiodynamic polarization values were -0.3 V and 0.3 V, relative to the stable OCP, respectively. A scan rate of 1.0 mV/s was used. The corrosion current density $i_{cor}$, corrosion potential $E_{cor}$, anodic Tafel slope $b_a$, and cathodic Tafel slope $b_c$ were obtained. The corrosion inhibition efficiency ($\eta_p$(%)) of CEF for mild steel and its coverage ($\theta_P$) on the steel surface were calculated as [27, 28]

$$\theta_P = 1 - i_{cor} / i_{cor}^0 \quad (1)$$

$$\eta_P(\%) = \theta_P \times 100\% \quad (2)$$

where $i_{cor}^0$ and $i_{cor}$ are the corrosion current density of mild steel in solutions without and with CEF inhibitor, respectively.

EIS measurements were obtained at a stable OCP. The excitation signal was a sine wave with amplitude of 10 mV and the frequency range was from 100 kHz to 0.01 Hz. Zview software was used to analyze the EIS data. The geometric coverage ($\theta_Z$) of CEF on mild steel surface was determined by the following expression [28-30]

$$\theta_Z = 1 - R_{ct}^0 / R_{ct} \quad (3)$$

where $R_{ct}^0$ and $R_{ct}$ are the charge transfer resistances of mild steel in solutions without and with CEF inhibitor, respectively. The inhibition efficiency ($\eta_Z(\%)$) was calculated as follows

$$\eta_Z(\%) = \theta_Z \times 100\% \quad (4)$$

To ensure the reliability of the test results, each group of samples was measured in parallel more than three times. All of the referenced potentials are relative to SCE.

### *2.3 Corrosion surface observations*

The morphologies of mild steel samples that were immersed in corrosive solutions in the absence and presence of CEF inhibitor for various time periods were analyzed via scanning electron microscopy (EVO-18).

## 3. RESULTS AND DISCUSSION

### *3.1 Open circuit potential*

Equilibration of the adsorption and desorption of organic molecules on the metal surface takes time. A film forms on the metal surface during this process. The OCP reflects the process by which the metal transitions from an unstable state to a stable state. However, the solution composition, ion and molecule adsorption-desorption processes, and disturbance of the solution can change the OCP values.

Figure 2 shows the OCP of mild steel in 1.0 mol/L $H_3PO_4$ and 0.6 mol/L NaCl solutions with various concentrations of CEF. As shown in Fig. 2a, in the absence of CEF in $H_3PO_4$ solution, the OCP value of mild steel increases rapidly at first. This is followed by a slow increase as the corrosion time increases further and stabilization after approximately 1 h. When CEF was added to the $H_3PO_4$ solution, the OCP is further enhanced and stabilizes more quickly. The OCP increases alongside the CEF concentration. The CEF molecules adsorbed onto the mild steel surface in 1.0 mol/L $H_3PO_4$ solution saturate quickly, leading to a fast thermodynamic equilibration of the metal surface.

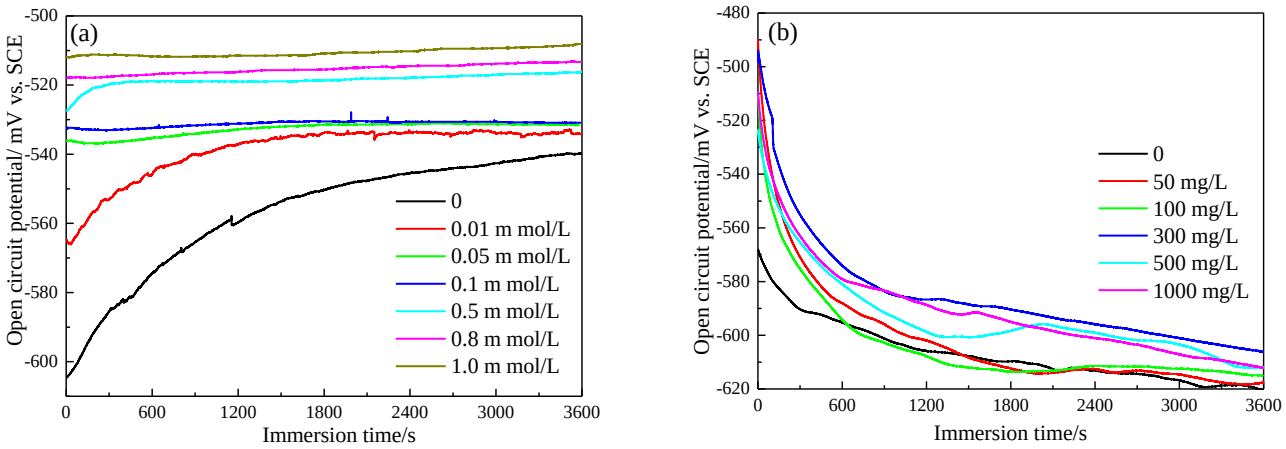


**Figure 2.** The OCP of mild steel in (a) 1.0 mol/L $H_3PO_4$ solution and (b) 0.6 mol/L NaCl solution with various amount of CEF.

As shown in Fig. 2b, the OCP of mild steel first decreases rapidly and then declines slowly regardless of whether CEF was added to the 0.6 mol/L NaCl solution. This trend is the opposite of that observed for the $H_3PO_4$ solution. Moreover, there is no obvious link between the change in the CEF concentration and the change in the OCP in NaCl solution.

As shown in Fig. 2, the addition of the CEF inhibitor leads to higher stable OCPs in both $H_3PO_4$ and NaCl solutions. However, the difference is less than 40 mV. It is thought that the CEF inhibitor does not change the corrosion mechanisms of mild steel in either solution [24, 31, 32].

It should be pointed out that the manner in which the OCP of mild steel varies with immersion time is different for the two solutions. This may be directly related to the different corrosion mechanisms of mild steel in acidic and neutral solutions, i.e., hydrogen evolution and oxygen corrosion, respectively.

In an acidic $H_3PO_4$ solution, the corrosion cell forms on the heterogeneous areas of the mild steel surface. The following oxidation reaction of iron takes place:

$$Fe \rightarrow Fe^{2+} + 2e^- \quad (5)$$

$$Fe \rightarrow Fe^{3+} + 3e^- \quad (6)$$

$$Fe^{2+} \rightarrow Fe^{3+} + e^- \quad (7)$$

Phosphoric acid is ionized multiple times, forming phosphate ions and $H^+$:

$$H_3PO_4 \rightarrow H_2PO_4^- + H^+ \quad (8)$$

$$H_2PO_4^- \rightarrow HPO_4^{2-} + H^+ \quad (9)$$

$$HPO_4^{2-} \rightarrow PO_4^{3-} + H^+ \quad (10)$$

The phosphate ions, because of strong coordination abilities, react with $Fe^{2+}$ and $Fe^{3+}$ and form soluble complexes such as $[Fe(PO_4)_2]^{3-}$ and $[Fe(HPO_4)_2]^-$. In addition, insoluble compounds such as $Fe_3(PO_4)_2$ and $FePO_4$ are formed and cover the mild steel surface [33, 34]. Furthermore, $H^+$ is reduced at the micro cathode sites:

$$2H^+ + 2e^- \rightarrow H_2 \uparrow \quad (11)$$

As mentioned above, the competition of the active dissolution and inhibition dissolution processes occur in an acidic solution. The gradual stabilization of the OCP indicates that the dissolution inhibition is dominant.

When CEF was added to the $H_3PO_4$ solution, the OCP of mild steel stabilizes rapidly and is less negative. This can be attributed to the adsorption of the CEF inhibitor on the surface of mild steel [12-27, 34]. In $H_3PO_4$ solution, the surface of mild steel is negatively charged because of the adsorption of $PO_4^{3-}$, $HPO_4^{2-}$, and $H_2PO_4^-$. The CEF molecules contain several hydrophilic functional groups, such as —$NH_2$, —CO—, and heteroatoms of N and S in five- and six-membered rings. These hydrophilic groups combine with $H^+$ on one end to form positively charged protonation products. They are subsequently electrostatically adsorbed to the negatively charged metal surface. These hydrophilic groups can combine with water molecules via hydrogen bonding. Moreover, the carboxylic acid functional group —COONa in the CEF molecules first dissociates into —COO— and then coordinates with $Fe^{2+}$ and $Fe^{3+}$. Lone pair electrons are present on the N and S heteroatoms in the five- and six-membered rings. They can also coordinate with iron to form coordination compounds. Hence, multiple ligands such as the carboxyl group, the amino group, and N and S heteroatoms chelate with the same iron ion ($Fe^{2+}$ or $Fe^{3+}$), forming stable polydentate chelates that are arranged in an ordered manner on the mild steel surface. In addition, a hydrophobic barrier layer forms on the surface of mild steel because of the hydrophobic groups of —$OCH_3$ and —$CH_2OCOCH_3$ in the CEF molecules. This hydrophobic barrier layer not only protects the metal matrix from $H_3O^+$ corrosion but also slows the diffusion of metal ions from the surface to the solution, which retards the charge transfer and ion diffusion between the metal/solution interfaces.

According to Hackerman theory [35, 36], the electrostatic adsorption and hydrogen bonding of the hydrophilic groups in the CEF molecules to the metal surface occur via physical adsorption, while the coordination bonding between the metal and N, S, and O in the CEF molecules occurs via chemical adsorption. Therefore, in $H_3PO_4$ solution, the CEF molecules are adsorbed on the surface of mild steel via a mixed adsorption mechanism, i.e., by both physical and chemical adsorption.

In a neutral NaCl solution, corrosion cells are also present on the inhomogeneous micro zones of mild steel. The anodic oxidation reactions of the metal occur according to Equations (1)–(3), and the cathodic reduction reaction of oxygen is as follows:

$$O_2 + 2H_2O + 4e^- \rightarrow 4OH^- \quad (12)$$

A series of chemical or electrochemical reactions between the reaction products then occurs:

$$Fe^{2+} + 2OH^- \rightarrow Fe(OH)_2 \downarrow \quad (13)$$

$$Fe^{3+} + 3OH^- \rightarrow Fe(OH)_3 \downarrow \quad (14)$$

$$Fe(OH)_2 \rightarrow FeO + H_2O \quad (15)$$

$$2Fe(OH)_3 \rightarrow Fe_2O_3 + 3H_2O \quad (16)$$

$$6FeO + O_2 \rightarrow 2Fe_3O_4 \quad (17)$$

The above reaction products are thus deposited on the surface of mild steel, impeding corrosion.

However, a large quantity of active chloride ions are adsorbed on the surface of mild steel in 0.6 mol/L NaCl solution. This limits $OH^-$ adsorption, hindering the formation of the protective products described by Equations (13)–(17). Moreover, the chloride ions react with the protective products to form a loose, flocculent Fe-O-Cl compound.

For the above reasons, mild steel in the neutral NaCl solution remains at an active dissolution state. Therefore, the OCP decreases when the corrosion proceeded, remaining unstable OCP after 1 h. Similarly, the adsorption of CEF molecules to the mild steel surface is drastically weakened or even prevented because of the preferential adsorption of the active chloride ions. Therefore, CEF has minimal influence on the OCP of mild steel (Fig. 2b).

### *3.2 Polarization measurements*

Figure 3 shows potentiodynamic polarization curves of mild steel in 1.0 mol/L $H_3PO_4$ and 0.6 mol/L NaCl solutions without and with CEF inhibitor. The corresponding polarization parameters are listed in Tables 1 and 2.

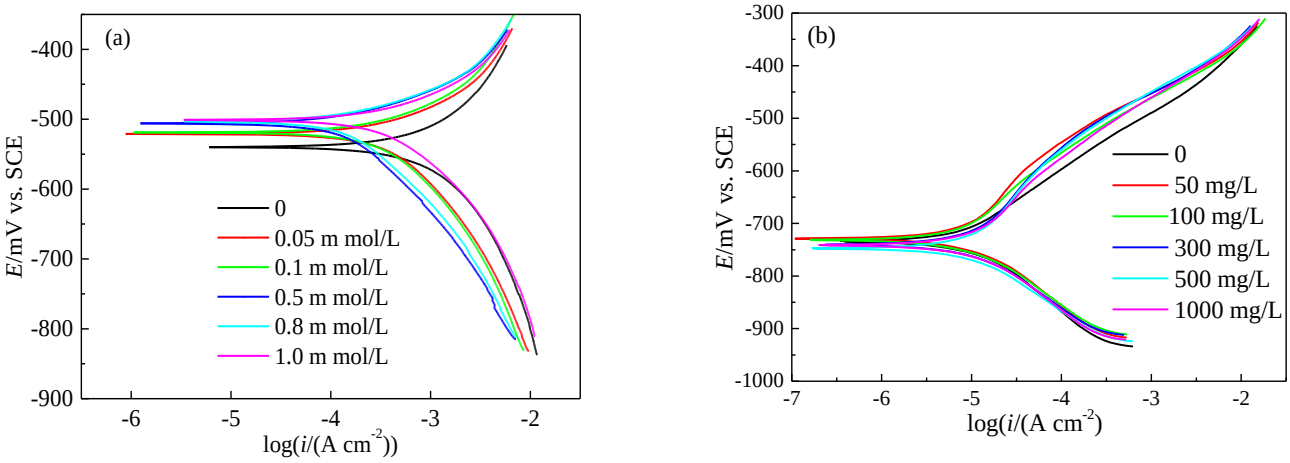


**Figure 3.** Polarization curves of mild steel in (a) 1.0 mol/L $H_3PO_4$ and (b) 0.6 mol/L NaCl solutions in the absence and presence of CEF inhibitor.

**Table 1.** Effect of CEF content on polarization parameters for mild steel in 1.0 mol/L $H_3PO_4$ solution.

| CEF concentration (m mol/L) | $E_{corr}$(mV) | $\beta_c$(mV/dec) | $\beta_a$(mV/dec) | $i_{corr}$(×$10^4$)(A $cm^{-2}$) | $\eta_p$(%) | $\theta_P$ |
|---|---|---|---|---|---|---|
| 0 | -540 | -186 | 180 | 6.32 | — | — |
| 0.05 | -521 | -163 | 153 | 1.81 | 71.4 | 0.714 |
| 0.10 | -519 | -161 | 153 | 1.43 | 77.4 | 0.774 |
| 0.50 | -506 | -142 | 125 | 0.78 | 87.7 | 0.877 |
| 0.80 | -503 | -137 | 138 | 0.84 | 86.7 | 0.867 |
| 1.00 | -501 | -142 | 147 | 1.31 | 79.3 | 0.793 |

As shown in Fig. 3a, when the CEF inhibitor was added to the 1.0 mol/L $H_3PO_4$ solution, the anodic and cathodic polarization current decrease and there is a slight positive shift in the corrosion potential. This suggests that both the anodic and cathodic corrosion processes of mild steel in 1.0 mol/L $H_3PO_4$ solution are inhibited by CEF, with a more significant effect for the anodic process. As the CEF concentration increases, the cathodic polarization curves are first markedly left-shifted and then right-shifted. The anodic polarization current first decreases substantially and then stabilizes. The cathodic and anodic currents are minimized when the CEF concentration was 0.5 m mol/L and 0.8 m mol/L, respectively.

**Table 2.** Effect of CEF content on polarization parameters for mild steel in 0.6 mol/L NaCl solution.

| CEF concentration (mg/L) | $E_{corr}$(mV) | $\beta_c$(mV/dec) | $\beta_a$(mV/dec) | $i_{corr}$(×10$^6$)(A cm$^{-2}$) | $\eta_p$(%) | $\theta_P$ |
|---|---|---|---|---|---|---|
| 0 | -734 | 138 | 117 | 5.64 | — | — |
| 50 | -729 | 132 | 204 | 5.17 | 8 | 0.08 |
| 100 | -731 | 123 | 158 | 5.04 | 11 | 0.11 |
| 300 | -740 | 121 | 207 | 4.92 | 13 | 0.13 |
| 500 | -747 | 115 | 215 | 5.17 | 8 | 0.08 |
| 1000 | -741 | 128 | 188 | 5.21 | 8 | 0.08 |

In $H_3PO_4$ solution, all of the anodic and cathodic polarization parts are nearly parallel (Fig. 3a). Therefore, there is minimal change in $\beta_c$ and $\beta_a$. This indicates that the anode and cathode reactions of mild steel are unchanged by the CEF inhibitor and only the corrosion rate decreases. The CEF molecules are influenced by the geometric coverage effect. The corrosion mechanism of mild steel does not change. This is in good agreement with the OCP results.

As shown in Table 1, as the CEF concentration increases, the $i_{cor}$ of mild steel in 1.0 mol/L $H_3PO_4$ solution first decreases substantially and then increases slightly, while $\eta_p$ and $\theta_P$ exhibit the opposite trend. The electrochemical indexes are optimal when the CEF concentration was in the range of 0.5 m mol/L and 0.8 m mol/L. This may be because a larger CEF concentration leads to a rearrangement of the molecules on the steel surface, resulting in additional susceptibility to corrosion via molecular gaps [37, 38].

A corrosion inhibitor can be considered anodic or cathodic only when the change in the corrosion potential $\Delta E_{cor}$ exceeds 85 mV [18, 27, 34, 38]. As shown in Table 1, the positive displacement of $E_{cor}$ for mild steel is less than 40 mV after CEF was added to the 1.0 mol/L $H_3PO_4$ solution. This implies that CEF is a mixed inhibitor with more of an effect on anodic corrosion than on cathodic corrosion.

As shown in Fig. 3b, the cathodic polarization branches are nearly unchanged when CEF was added to the 0.6 mol/L NaCl solution. The anode current declines slightly and CEF can only marginally delay anode corrosion. $E_{cor}$, $\beta_c$, and $\beta_a$ are almost unchanged by CEF (Table 2). Furthermore, the $\theta_P$ of the CEF molecules is only about 0.10. This suggests that the inhibition efficiency of CEF for mild steel in 0.6 mol/L NaCl is limited.

An organic inhibitor can adsorb on a metal surface via its N, O, and S heteroatoms and organo functional groups. In an acidic $H_3PO_4$ solution, the amino functional groups in the CEF molecules are protonated and adsorbed on the anode sites of the metal surface. The oxygen atoms in the aliphatic chain can also adsorb on the anode sites [38-40]. Hence, the anode dissolution of the metal is controlled. In addition, multi-dentate ligands are formed via amino functional groups, carboxyl groups, and partial oxygen atoms in the CEF molecules that adsorb on the metal surface, impeding the partial anode reaction. Therefore, the anode current of mild steel is reduced. In a neutral NaCl solution, the CEF molecules are in the form of zwitterions, with a negative charge on the carboxyl groups and a positive charge on protonated amino groups [38, 41]. Corrosion inhibition of mild steel by CEF molecules in NaCl solution occurs because of CEF adsorption and deposition of corrosion products on the active sites, i.e., the geometric coverage effect. This depends on the properties of the CEF molecules and the stability of the metal surface [42]. However, in a 0.6 mol/L NaCl solution, most of the metal surface is covered with chloride ions, limiting the adsorption of CEF molecules on the active sites and thus dramatically weakening the corrosion inhibition efficiency of the CEF molecules.

*3.3 Corrosion morphology*

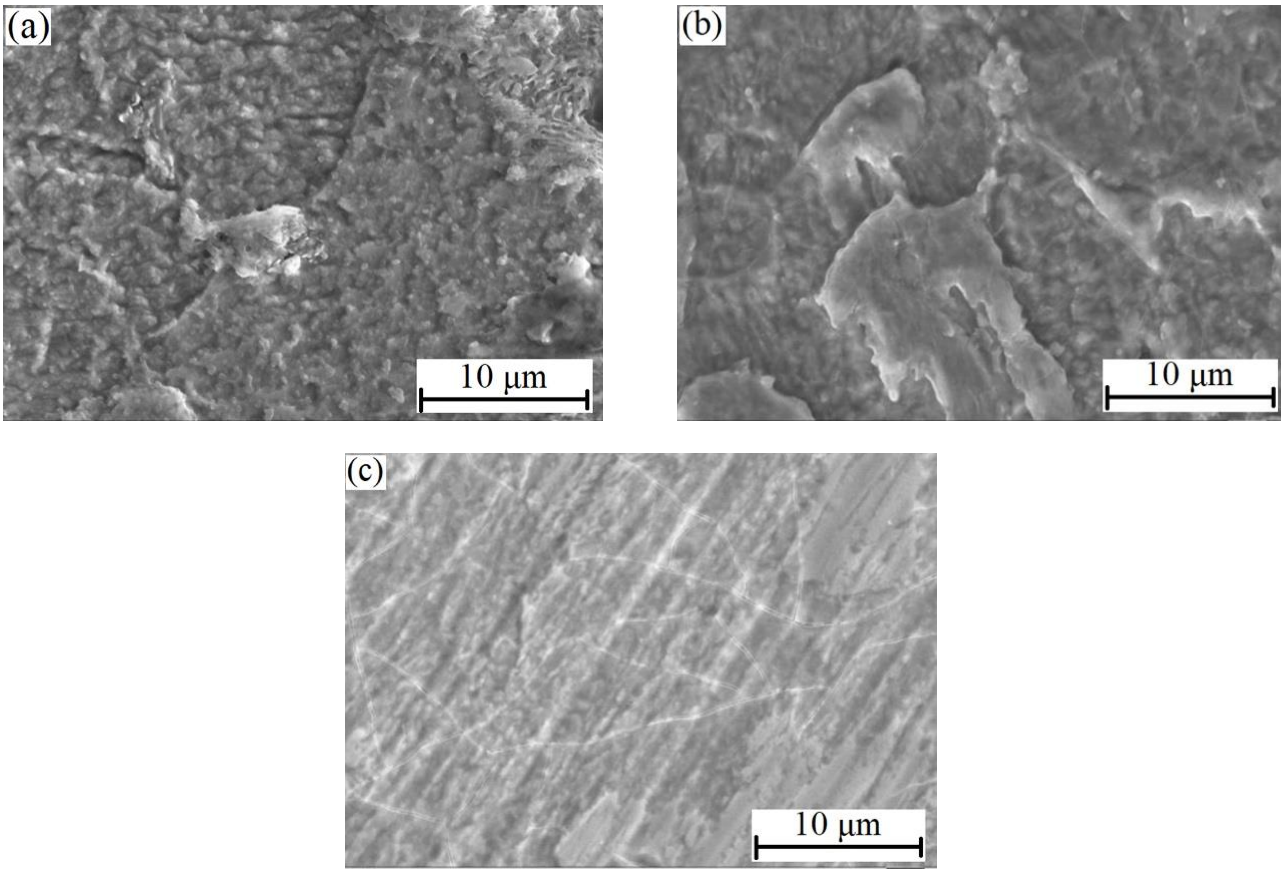


**Figure 4.** Surface morphologies of mild steel samples immersed in 1.0 mol/L $H_3PO_4$ solutions (a) without CEF, (b) with 0.5 mmol/L CEF, and (c) with 1.0 mmol/L CEF.

Figures 4 and 5 show the corrosion morphologies of mild steel immersed in 1.0 mol/L $H_3PO_4$ and 0.6 mol/L NaCl solutions for 1 h, respectively. As shown in Fig. 4a, in the absence of CEF in 1.0 mol/L $H_3PO_4$ solution, the corrosion products on the surface of mild steel are loose and coarse. In the presence of CEF, the density of the corrosion products improves and a continuous thin film covers the initial film (Fig. 4b). Upon increasing the CEF concentration, the compactness of the corrosion products is further enhanced and the outer film becomes more visible (Fig. 4c). However, a higher CEF concentration leads to cracks in the outermost thin film.

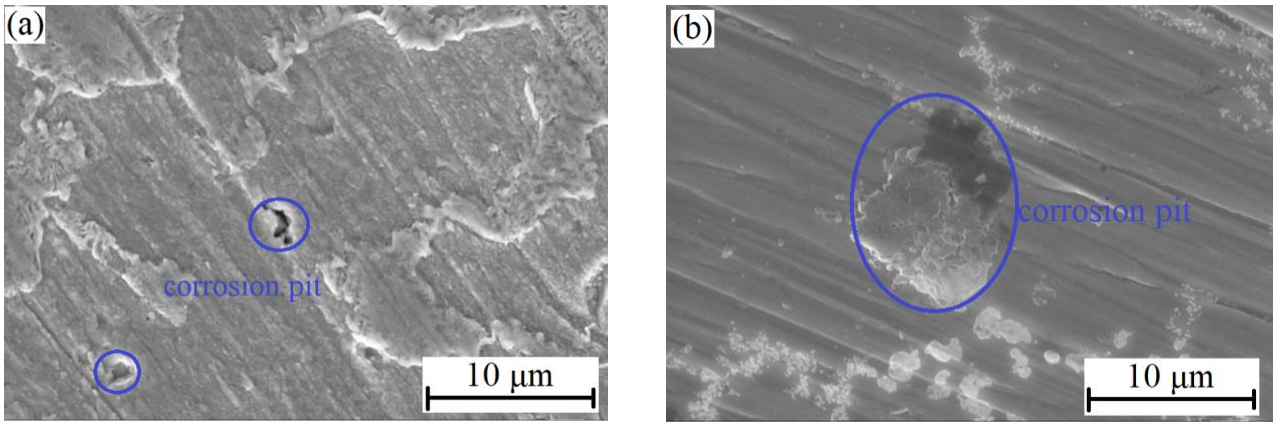


**Figure 5.** Corrosion morphologies of mild steel samples immersed in neutral 0.6 mol/L NaCl solutions (a) without CEF and (b) with CEF

In the absence of CEF, mild steel becomes severely corroded in 0.6 mol/L NaCl solution. A large number of pits appear in Fig. 5a. Loose corrosion products were rinsed off prior to imaging. In the presence of CEF, the number of pits decreases, but the pits that appear are deeper (Fig. 5b). These results are in good agreement with the OCP results and polarization measurements. The corrosion protection that CEF provides for mild steel in NaCl solution is quite limited.

*3.4 EIS measurements*

Figure 6 shows EIS curves for mild steel in 1.0 mol/L $H_3PO_4$ solution. Regardless of whether CEF was added, the shapes of the EIS curves are quite similar, with one high-frequency capacitance loop, one low-frequency capacitance loop, and a low-frequency of inductance loop. The first loop corresponds to the double-layer capacitance at the interface between the metal and solution, the second is related to adsorption on the metal surface, and the last can be attributed to metal dissolution [42, 43]. The consistency of the EIS shapes confirms that the corrosion mechanism for mild steel in 1.0 mol/L $H_3PO_4$ solution is consistent as well.

As shown in Fig. 6, the starting points of the real parts of the EIS diagrams are clearly larger than zero. The horizontal section of the high-frequency part of the log|$Z$| versus log$f$ plots is also substantially larger than zero. This can be attributed to the poor conductivity of the phosphoric acid solution. As the CEF concentration increases, the maximum impedance values in Nyquist plots and the

low-frequency impedances in Bode diagrams first increase significantly and then decrease. Therefore, the electrochemical impedance and corrosion resistance trends of mild steel are the same.

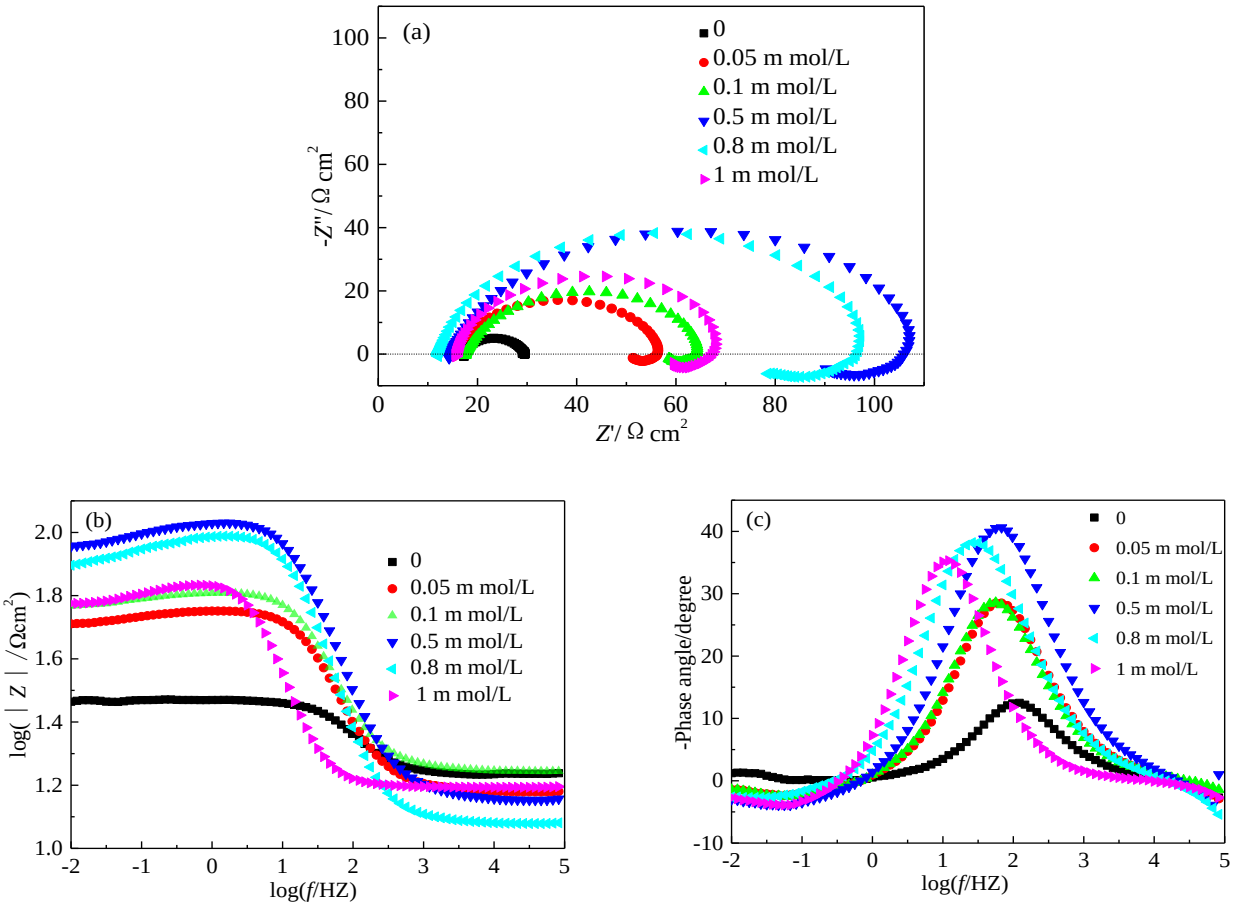


**Figure 6.** EIS curves of mild steel in 1.0 mol/L $H_3PO_4$ solution with various CEF concentrations, (a) Nyquist diagrams and (b) and (c) Bode diagrams.

The equivalent circuit in Fig. 7 was used to analyze the EIS diagrams [42-44]. $R_s$ is the solution resistance, $CPE_{dl}$ is the double-layer capacitance at the interface between metal and solution, $R_{ct}$ is the charge transfer resistance on the steel surface.

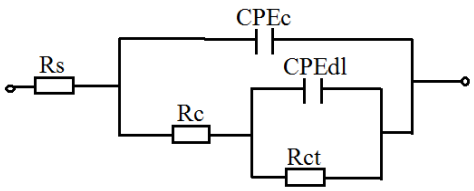


**Figure 7.** Equivalent circuit used to analyze the EIS diagrams.

In the actual system, a dispersion of frequency response was observed for the double-layer capacitance because of the heterogeneity of the chemical composition and the roughness of the metal

surface [39-44]. Hence, the circular center of the capacitance loop deviates from the real axis and the peak of the negative phase angle is smaller than 90° (Figs. 6a and 6c). The constant phase angle element (CPE) is used to characterize the double-layer capacitance and is expressed as:

$$Z_{CPE}=1/(Y_0(j\omega)^n) \quad (18)$$

where $Y_0$ is the auxiliary parameter related to the capacitance value, $\omega$ is the angular frequency, $j$ is the imaginary root, and $n$ is the degree of capacitance distortion. A larger $n$ indicates that the real capacitance is closer to the ideal capacitance for a surface with a lower roughness and a higher density.

Figure 8 shows a comparison of the fitted and experimental results. The fitting is in good agreement with the experimental results and the error is less than 5%. Hence, the proposed equivalent circuit is realistic.

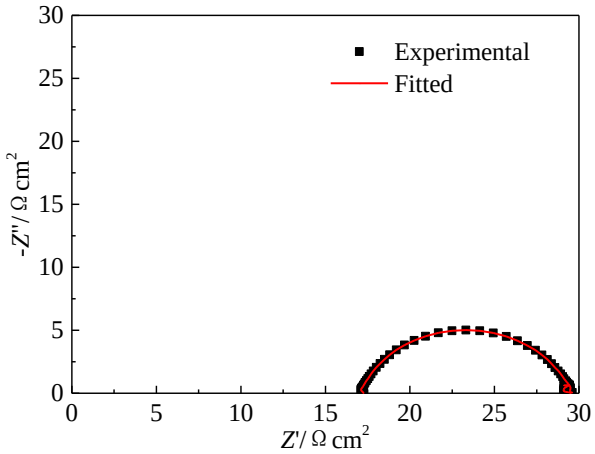


**Figure 8.** Comparison of experimental and fitted EIS results.

The parameters obtained by fitting the EIS data for mild steel in 1.0 mol/L $H_3PO_4$ solution are listed in Table 3. $R_s$ of phosphoric acid is high and its conductivity is poor. In the presence of CEF inhibitor, $R_s$ is almost unchanged. $R_{ct}$ and $n_{dl}$ increase markedly but $Y_{0\text{-dl}}$ decrease. These results can all be attributed to adsorption of CEF molecules, which delays oxidation of mild steel and reduction of hydrogen ions. This enhances the charge transfer resistance. Moreover, the adsorption of CEF molecules results in formation of a CEF thin film, which improves the surface uniformity of mild steel (Fig. 4). Therefore, the double-layer capacitance is closer to the plate capacitance and $n_{dl}$ is closer to 1. According to Helmholtz model, the capacitance can be expressed as [45, 46]:

$$C=\varepsilon S/(4\pi kd) \quad (19)$$

where $\varepsilon$ is the dielectric constant, $S$ is the area of the capacitance plate, $d$ is the distance between plates, and $k$ is the electrostatic constant. Therefore, a decrease in $Y_{0\text{-dl}}$ may be related to a decrease in the dielectric constant or the plate area, or an increase in the distance between the two plates. After CEF was added, the CEF molecules can replace water molecules and adsorb on the surface of mild steel, resulting in a lower dielectric constant. The dielectric constant of the water molecules is larger than those of other molecules [39, 41]. Formation of an adsorbed CEF film on the surface of mild steel can

lead to a decrease in its roughness and an increase in its density. Therefore, the total surface area decreases and the two plates' distance increases.

**Table 3.** Parameters fitted from EIS data for mild steel in a 1.0 mol/L H3PO4 solution with various CEF concentrations

| CEF concentration (m mol/L) | $R_s$(Ω cm$^2$) | $Y_{0\text{-dl}}$(×10$^4$) (Ω$^{-1}$·cm$^{-2}$·s$^{-n}$) | $n_{dl}$ | $R_{ct}$(Ω·cm$^2$) | $\eta_Z$(%) | θz |
|---|---|---|---|---|---|---|
| 0 | 17.12 | 3.63 | 0.8645 | 12.33 | — | — |
| 0.05 | 15.19 | 2.54 | 0.8564 | 42.27 | 70.83 | 0.7083 |
| 0.10 | 14.79 | 1.90 | 0.8734 | 51.94 | 76.26 | 0.7626 |
| 0.50 | 14.41 | 1.65 | 0.8930 | 96.11 | 87.17 | 0.8717 |
| 0.80 | 14.75 | 1.56 | 0.9098 | 87.15 | 85.85 | 0.8585 |
| 1.00 | 17.14 | 2.03 | 0.9465 | 58.28 | 78.84 | 0.7884 |

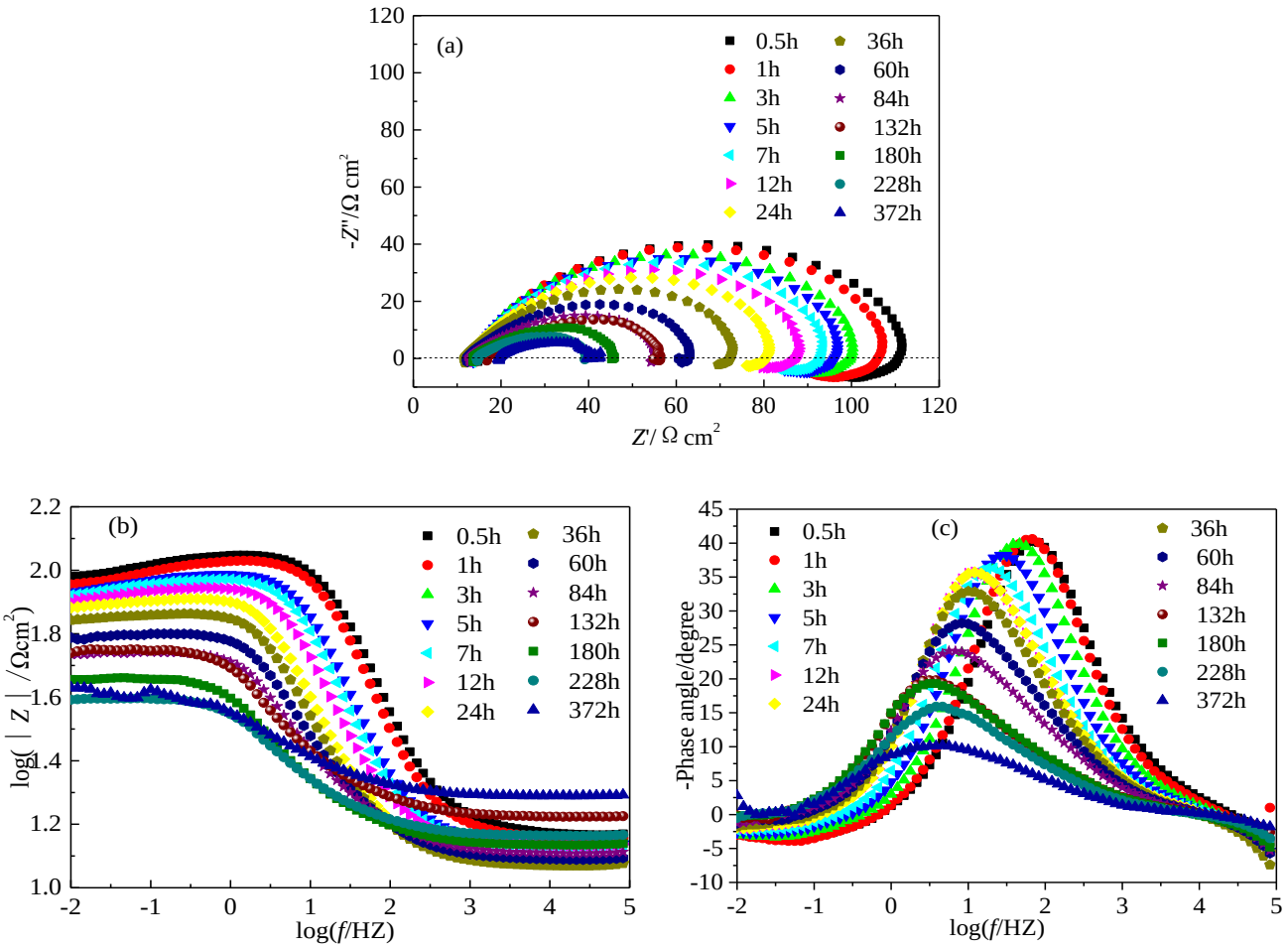


**Figure 9.** EIS diagrams of mild steel immersed in 1.0 mol/L $H_3PO_4$ solution for different durations (a) Nyquist and (b) and (c) Bode diagrams.

As shown in Table 3, as the CEF concentration increases, the $Y_{0\text{-dl}}$ first decreases and then increases. The changes $R_{ct}$, $\theta_Z$, and $\eta_Z$ exhibit the opposite trend. The inhibition efficiency is optimal when the CEF concentration is in the range of 0.5 m mol/L and 0.8 m mol/L. This is in good agreement with the results of the polarization and OCP measurements.

### *3.5 Time effectiveness of CEF inhibitor for mild steel in 1.0 mol/L $H_3PO_4$ solution*

The long-term corrosion inhibition effectiveness of CEF for mild steel in 1.0 mol/L $H_3PO_4$ solution was also evaluated. EIS diagrams with immersion times of 0.5 h–372 h are shown in Fig. 9 and the corresponding fitted parameters are listed in Table 4.

The shape of the Nyquist diagram changes little with the immersion time, although the impedance size gradually decreases. The low-frequency impedance and the peak of the negative phase angle in the Bode diagrams decrease. Moreover, the frequency that corresponds to the oblique line segment in Fig. 9b and the peak of the negative phase angle are shifted towards a lower frequency. This indicates a decrease in $R_{ct}$ and an increase in $Y_{0\text{-dl}}$ (Table 4). Moreover, as the corrosion time increases, a decrease in $n_{dl}$ and an increase in $Y_{0\text{-dl}}$ imply an increase in the roughness of the double-layer capacitance. This can be seen from the SEM images in Fig. 10. It suggests that CEF-based corrosion inhibition of mild steel in 1.0 mol/L $H_3PO_4$ solution is effective over extended periods. The $R_{ct}$ value for mild steel in 1.0 mol/L $H_3PO_4$ solution after corrosion for 372 h in the presence of CEF is significantly higher than that for the sample without CEF after corrosion for only 1 h.

**Table 4.** EIS parameters for mild steel immersed in 1.0 mol/L $H_3PO_4$ solution with CEF for different time.

| Immersion time (h) | $R_s$(Ω cm$^2$) | $Y_{0\text{-dl}}$(×10$^4$) (Ω$^{-1}$·cm$^{-2}$·s$^{-n}$) | $n_{dl}$ | $R_{ct}$(Ω·cm$^2$) | $\eta_Z$(%) | $\theta_Z$ |
|---|---|---|---|---|---|---|
| 0.5 | 14.89 | 1.52 | 0.8401 | 100.31 | 87.71 | 0.8771 |
| 1 | 14.41 | 1.65 | 0.8530 | 96.11 | 87.17 | 0.8717 |
| 3 | 12.59 | 2.40 | 0.8511 | 89.57 | 86.23 | 0.8623 |
| 5 | 12.50 | 3.00 | 0.8463 | 86.25 | 85.70 | 0.8570 |
| 7 | 13.52 | 3.69 | 0.8384 | 83.16 | 85.17 | 0.8517 |
| 12 | 14.60 | 5.30 | 0.8289 | 77.41 | 84.07 | 0.8407 |
| 24 | 12.14 | 8.98 | 0.7948 | 73.10 | 83.13 | 0.8313 |
| 36 | 11.85 | 12.15 | 0.7653 | 65.20 | 81.09 | 0.8109 |
| 60 | 12.37 | 18.18 | 0.7243 | 54.87 | 77.53 | 0.7753 |
| 84 | 12.95 | 24.93 | 0.6965 | 45.36 | 72.82 | 0.7282 |
| 132 | 12.88 | 39.36 | 0.6688 | 42.71 | 71.13 | 0.7113 |
| 180 | 13.84 | 47.03 | 0.6772 | 33.57 | 63.27 | 0.6327 |
| 228 | 14.70 | 53.04 | 0.6687 | 25.53 | 51.70 | 0.5170 |
| 372 | 19.35 | 86.64 | 0.5814 | 23.62 | 47.80 | 0.4780 |

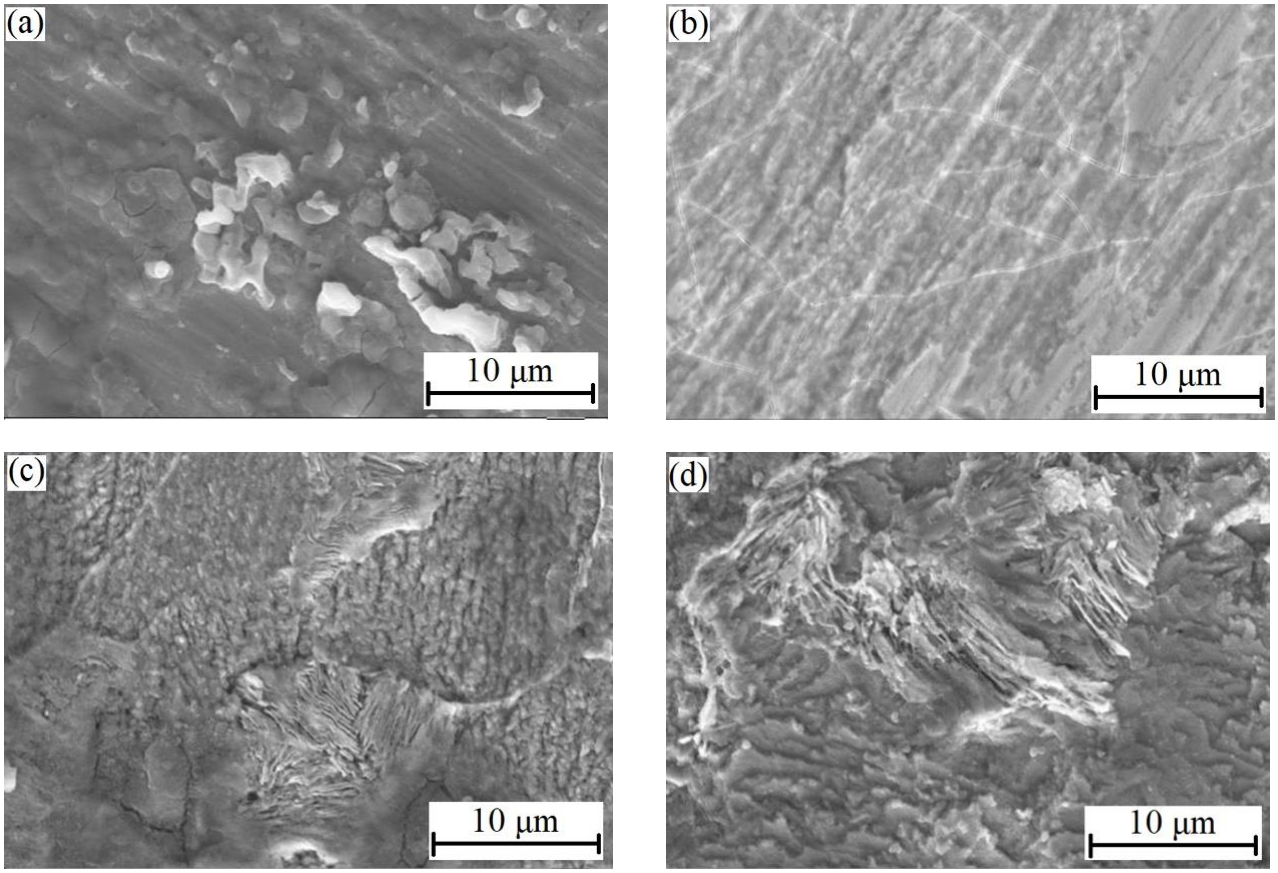


**Figure 10.** SEM morphologies of mild steel samples immersed in 1.0 mol/L H3PO4 solution for various durations: (a) 0.5 h; (b) 1 h; (c) 7 h; and (d) 168 h

*3.6 Adsorption mechanism of CEF on mild steel in 1.0 mol/L $H_3PO_4$ solution*

Corrosion inhibition by organic inhibitors is closely related to the adsorption behavior. CEF-based corrosion inhibition of mild steel in 1.0 mol/L $H_3PO_4$ solution was fitted using various adsorption isotherm equations. The adsorption of CEF can be described by Langmuir adsorption equation [34, 39, 44]:

$$c/\theta = c + 1/K \quad (20)$$

where $c$ is the CEF concentration (mol/L), $K$ is the adsorption equilibrium constant (L/mol), and $\theta$ is the inhibitor coverage on the mild steel surface.

The $c/\theta_Z$~$c$ line (Fig. 11) was plotted based on the fitted EIS parameters and Equation (20). Linear regression was performed, generating a linear correlation coefficient (R) of 0.997. Hence, the Langmuir adsorption equation can be used to model the data, indicating that the adsorption film on the surface of mild steel is a monolayer [46, 47]. And $K$ is about $112.19\times10^3$ L/mol, determined according to the line intercept.

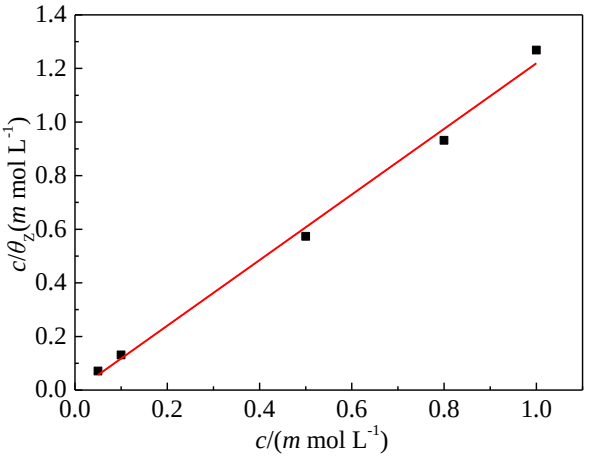


**Figure 11.** Langmuir adsorption line of the CEF inhibitor on mild steel surface in 1.0 mol/L $H_3PO_4$ solution.

The thermodynamic adsorption parameters are important to explain the micro adsorption behaviors of the inhibitors on the surface of mild steel. The relationship between the standard $K$ of the inhibitor on the metal surface and the standard Gibbs free energy ($\Delta G^0$) can be expressed as [47-49]:

$$K = \frac{1}{\rho_{\text{solvent}}} \exp\left(\frac{-\Delta G^0}{RT}\right) \tag{21}$$

where $\rho_{\text{solvent}}$ is the molar concentration of $H_2O$ in the phosphoric acid solution (~55.5 mol/L), $R$ is the gas constant (8.314 J/(mol·K)), and $T$ is the thermodynamic temperature (K). The $\Delta G^0$ value is approximately -38.76 kJ/mol. A negative $\Delta G^0$ value indicates that adsorption of CEF on the mild steel surface is spontaneous.

Typically, chemical adsorption occurs when $\Delta G^0$ is smaller than -40 kJ/mol, while physical adsorption occurs when $\Delta G^0$ is larger than -20 kJ/mol [48-50]. Chemical adsorption includes sharing of electrons between iron atoms and inhibitor molecules or formation of covalent bonds due to charge transfer. Physical adsorption involves electrostatic interactions between the inhibitor molecules and the metal surface. The $\Delta G^0$ value (-38.76 kJ/mol) of CEF on the mild steel surface suggests that adsorption of CEF on the mild steel surface in 1.0 mol/L $H_3PO_4$ solution occurs via a mixed adsorption mechanism, with chemical adsorption dominating and a smaller contribution provided by physical adsorption. CEF can be physically adsorbed onto the mild steel surface via electrostatic adsorption and hydrogen bonding. It can also be chemically adsorbed via formation of extremely stable polydentate chelates, which play an important role in corrosion protection.

## 4. CONCLUSIONS

The expired antibiotic cefotaxime sodium (CEF) was used as a corrosion inhibitor for mild steel in 1.0 mol/L $H_3PO_4$ solution and 0.6 mol/L NaCl solution (acidic and neutral media, respectively). The corrosion behavior was investigated via OCP, polarization, and EIS measurements. The adsorption isotherm equation and thermodynamic parameters were analyzed and the inhibition

mechanism was discussed. Finally, the differences between corrosion results in the two solutions were explained. The main conclusions are as follows:

(1) In $H_3PO_4$ solution, a dynamic equilibrium of the adsorption and desorption processes of CEF molecule was reached rapidly on the mild steel surface and a stable OCP was quickly obtained. However, it was difficult in NaCl solution.

(2) In $H_3PO_4$ solution, a continuous and compact thin film was formed and CEF acted as a mixed inhibitor that mainly controlled anodic corrosion. Electrochemical indexes improved with increasing CEF concentration. The optimum CEF concentration was in the range of 0.5 m mol/L and 0.8 m mol/L; and the CEF adsorption coverage was 0.87.

(3) However, in NaCl solution, CEF molecules only slightly inhibited anodic corrosion. The CEF coverage was only about 0.1. A large number of corrosion pits were still present and the inhibition efficiency was poor.

(4) CEF molecules could provide long-term corrosion protection for mild steel in $H_3PO_4$ solution. The thin film eventually desorbed and the charge transfer resistance gradually decreased. However, the charge transfer resistance of mild steel immersed in $H_3PO_4$ solution with CEF for 372 h (about 23.62 $\Omega$ $cm^2$) was still markedly larger than that of a sample in $H_3PO_4$ solution without CEF that was corroded for only 1 h (12.3 $\Omega$ $cm^2$).

(5) Adsorption of CEF molecules on the mild steel surface in $H_3PO_4$ solution was best described by Langmuir adsorption isotherm. The $\Delta G^0$ value was approximately -38 kJ/mol. A mixed adsorption mode was identified, but chemical adsorption was dominant. The inhibition differences between both solutions were directly related to the different corrosion mechanisms and the large quantity of chloride ions.

ACKNOWLEDGMENTS

This work was supported by the Natural Science Foundation of Fujian Province (No. 2017J01489), the National Natural Science Foundation of China (No. 51778247), and the Program for the Innovative Research Team in Science and Technology in Fujian Province University.

## References

1. C. C. Yin, X. L. Ban, Y. Wang, J. T. Zhang, L. Fan, R. Cai and J. P. Zhang, *Int. J. Electrochem. Sci*., 14 (2019) 11152.
2. E. I. Khlusova, V. V. Orlov, *Metallurgist*, 56 (2013) 684.
3. U. A. Fareeha, R. Bahgat, R. A. S. Nazal Naeem and S. Ahmed, *Surf. Coat. Technol.*, 372 (2019) 121.
4. J. Riskin, *Electrocorrosion Prot. Met.*, 179 (2008) 221.
5. S. Masroor, *J. Bio Tribo Corros.*, 3 (2017) 27.
6. V. N. Ayukayeva, G. I. Boiko, N. P. Lyubchenko, R. G. Sarmurzina and S. A. Dergunov, *Colloid. Surface A.*, 579 (2019) 123636.
7. F. B. Ma, Y. Zhang, H. J. Wang, W. H. Li and B. R. Hou, *Int. J. Electrochem. Sci.*, 13 (2018) 235.
8. C. Verma, E. E. Ebenso and M. A. Quraishi, *J. Mol. Liq.*, 248 (2017) 927.
9. C. Lai, J. Cao, Y. F. Deng, Y. F. Yang, X. Wen, Z. L. Wang, C. W. Fan, Y. N. Shi and Y. Li, *Int. J. Electrochem. Sci.*, 14 (2019) 10259.
10. R. K. Ahmed and S. T. Zhang, *Int. J. Electrochem. Sci.*, 14 (2019) 10657.

11. S. Hadisaputra, A. A. Purwoko, Rahmawati, D. Asnawati, Ilhamsyah, S. Hamdiani and Nuryono, *Int. J. Electrochem. Sci.*, 14 (2019) 11110.
12. H. H. Hassan, *Electrochim. Acta*, 52 (2007) 6359.
13. R. Guo, Y. P. Li, R. X. Tu, B. Song and Y. Guo, *Chemical J. Chinese U.*, 39 (2018) 1018.
14. I. Ahamad and M. A. Quraishi, *Corros. Sci.*, 51 (2009) 2006.
15. X. Zhang, J. X. Wen, Y. X. Liu and X. M. Yang, *Surf. Technol.,* 47 (2018) 231.
16. W. Chen, C. P. Guan, S. M. Yang and X. A. Hu, *J. Chin. Soc. Corr. Pro.*, 36 (2016) 177.
17. A. Singh, E. E. Ebenso and M. A. Quraishi, *Int. J. Corros.*, (2012) 1.
18. Z. Zhao, *Study of corrosion inhibition performance of two kinds of corrosion inhibitors based on organic drugs for Q235 carbon steel and aluminum alloy*, Beijing University of Chemical Technology, (2016) Beijing, China.
19. G. Gece, *Corros. Sci.*, 53 (2011) 3873.
20. S. B. Ade, N. V. Shitole and S. M. Lonkar, *J. Chem. Pharm. Res.*, 6 (2014) 1865.
21. G. Karthik and M. Sundaravadivelu, *J. Adhesion Sci. Technol.*, 31 (2017) 530.
22. R. S. Nathiya, S. Perumal, V. Murugesan and V. Raj, *J. Bio Tribo –Corros.*, 4 (2018) 4.
23. R. A. Anaee, I. H. R. Tomi, M. H. Abdulmajeed, S. A. Naser and M. M. Kathem, *J. Mol. Liq.*, 279 (2019) 594.
24. A. K. Singh, A. K. Pandey, P. Banerjee, S. K. Saha and G. Singh, *J. Environ. Chem. Eng.*, 7 (2019) 1027.
25. P. Dohare, D. S. Chauhan, A. A. Sorour and M. A. Quraishi, *Mater. Disc.*, 9 (2017) 30.
26. O. S. I. Fayomi, I. G. Akande, A. P. I. Popoola and H. Molifi, *J. Mater. Res. Technol.*, 8 (2019) 3088.
27. T. L. Zhang, S. R. Cao, S. S. Dai, W. C. Jiang and H. P. Quan, *Corros. Sci. Prot. Technol.*, 26 (2014) 329.
28. M.E. Mashuga, L.O. Olasunkanmi and E.E. Ebenso, *J. Mol. Struct.*, 1136 (2017) 127.
29. T.K. Chaitra, K.N. Mohana and H.C. Tandon, *Arab J. Basic Appl. Sci.*, 25 (2018) 45.
30. D.K. Singh, E.E. Ebenso, M.K. Singh, D. Behera, G. Udayabhanu and R.P. John, *J. Mol. Liq.*, 250 (2018) 88.
31. A.K. Satapathy, G. Gunasekaran, S.C. Sahoo, Kumar Amit and P.V. Rodrigues, *Corros. Sci.*, 51 (2009) 2848.
32. D. Jayaperumal, *Mater. Chem. Phys.*, 119 (2010) 478.
33. M. Messali, H. Lgaz, R. Dassanayake, R. Salghi, S. Jodeh, N. Abidi snd O. Hamed, *J. Mol. Struct.*, 1145 (2017) 43.
34. J. X. Liu, S. D. Deng, X. Xu and X. H. Li, *Corros. Sci. Prot. Technol.*, 30 (2018) 120.
35. M. T. Coltharp and N. Hackerman, *J. Colloid Interface Sci.*, 43 (1973) 176.
36. T. Murakawa, T. Kato, S. Nagaura and N. Hackerman. *Corros. Sci.*, 8 (1968): 483.
37. H. J. Huang, Z. Q. Wang, Y. L. Gong, F. Gao, Z. P. Luo, S. T. Zhang and H. R. Li, *Corros. Sci.*, 123 (2017) 339.
38. Z. Q. Wang, Y. L. Gong, C. Jing, H. J. Huang, H. R. Li, S. T. Zhang and F. Gao, *Corros. Sci.*, 113 (2016) 64.
39. H. Nady, *Egyptian J. Petroleum*, 26 (2017) 905.
40. M. Talebian, K. Raeissi, M. Atapour, B.M. Fernández-Pérez, Z. Salarvand, S. Meghdadi, M. Amirnasr and R.M. Souto, *Applied Surf. Sci.*, 447 (2018) 852.
41. C. N. Cao, *Principle of Electrochemical Corrosion*, Chemistry Industry Press, (2018) Beijing, China.
42. G. Bereket and A. Yurt, *Corros. Sci.*, 43 (2001) 1179.
43. M.Abdallah, M. Alfakeer, A. M. Alonazi and S. S. Al-Juaid, *Int. J. Electrochem. Sci.*, 14 (2019) 10227.
44. Y. J. Qiang, S. T. Zhang, S. Yan, X. F. Zou and S. J. Chen, *Corros. Sci.*, 126 (2017) 295.
45. T.H. Silva, V. Garcia-Morales, C. Moura, J.A. Manzanares and F. Silva, *Langmuir*, 21 (2015) 7461.

46. Caio Machado Fernandes, Thayssa da S. Ferreira Fagundes, Nazir Escarpini dos Santos, Talita Shewry de M. Rocha, Rafael Garrett, Ricardo Moreira Borges, Guilherme Muricy, Alessandra Leda Valverde, Eduardo Ariel Ponzio. *Electrochimi. Acta*, 312 (2019) 137.
47. Y. J. Qiang, S. T. Zhang, B. C. Tan and S. J. Chen, *Corros. Sci.*, 133 (2018) 6.
48. N. El Hamdani, R. Fdil, M. Tourabi, C. Jama and F. Bentiss, *Appl. Surf. Sci.*, 357 (2015) 1294.
49. A. Ghames, T. Douadi, S. Issaadi, L. Sibous, K.I. Alaoui, M. Taleba and S. Chafaa, *Int. J. Electrochem. Sci.*, 12 (2017) 4867.
50. Z. Hu, Y. Meng, X. Ma, H. Zhu, J. Li, C. Li and D. Cao, *Corros. Sci.*, 112 (2016) 563.